Submitted to the
International Conference on High Energy Physics
16-22 August 2004, Beijing, China

Abstract: 6-0248 **QCDsoft**

Exclusive electroproduction of ϕ mesons at HERA

ZEUS Collaboration

3 August 2004

Abstract

Exclusive electroproduction of ϕ mesons has been studied in $e^{\pm}p$ collisions with the ZEUS detector at HERA in the kinematic range $2 < Q^2 < 70\,\text{GeV}^2$ and $35 < W < 145\,\text{GeV}$ using an integrated luminosity of 66.4 pb^{-1}. The cross sections are presented as a function of Q^2, W, t and helicity angle θ_h. The results are consistent with a global vector meson production scaling with $Q^2 + M_V^2$. The W dependence was extracted in bins of t, and the results are consistent with no dependence on t. The ratio R of the cross sections for longitudinally and transversely polarized virtual photons, determined from the angular distribution of the decay products of the ϕ mesons, rises smoothly as a function of Q^2.

1 Introduction

The exclusive electroproduction of vector mesons (VMs) is a clean process that can be measured precisely in a large phase space. Precision data from this process can be used to challenge model predictions in a region that includes the transition between soft and hard dynamics.

A simple picture for the process $e\,p \to e\,pV$, where V represents a vector meson, can be formulated in the rest frame of the proton. In this frame, the virtual photon emitted from the scattered electron fluctuates into a quark-antiquark dipole, which then scatters elastically off the proton. Long after the interaction, the $q\bar{q}$ wave function collapses into a vector meson. It can be shown that, at high energy, the $q\bar{q}$ formation, scattering, and collapse into a VM are well separated in time and the cross-section can be factorized using the dipole cross-section on the proton [1]. For low values of photon virtuality (Q^2) and VM mass, large dipole sizes dominate and the interaction is expected to be described by Regge phenomenology [2] and the Vector Meson Dominance model (VMD). On the other hand, in the presence of a hard scale, perturbative QCD (pQCD) becomes applicable. In lowest order pQCD the process proceeds via the exchange of two gluons, and the production of vector mesons can be related to the gluon density in the proton. In the dipole model picture, the hard scale is provided by the small transverse separation of the $q\bar{q}$ pair. For the light vector mesons like ϕ and ρ it is expected that at small Q^2 the large dipoles dominate, while with increasing Q^2 a smooth transition towards pQCD predictions will occur. In the case of the J/ψ meson the hard scale is always present due to the large mass of the charm quarks.

The exclusive electroproduction of light (ρ, ω, ϕ) and heavy $(J/\psi, \psi', \Upsilon)$ vector mesons, $ep \to eVp$, has been investigated previously at HERA [3–21]. The increased precision of the recent data allows the study of the dependence of this process on the different scales involved: the mass squared of the vector meson, M_V^2, the square of the centre-of-mass energy of the photon-proton system, W^2, the exchanged-photon virtuality, Q^2, and the four-momentum transfer squared at the proton vertex, t.

The energy dependence of the $\gamma^* p$ cross section is a good indicator of whether a hard scale is present or not. Data from exclusive ρ production [4–6] show that the cross section $\sigma(\gamma^* p \to \rho p)$ rises with W as W^δ, where δ increases with Q^2 from about 0.2 at $Q^2 = 0$ (photoproduction) to about 0.7 at $Q^2 \approx 30\,\mathrm{GeV}^2$. However, in the case of exclusive J/ψ production the cross section rises steeply with W even for photoproduction [3,10,13]. It is therefore interesting to investigate ϕ production since it represents an intermediate mass scale.

In this paper, the preliminary results from a study of exclusive ϕ production are presented. The data collected during 1998-2000 with the ZEUS detector correspond to an integrated luminosity of 15.06 pb^{-1} for e^-p and 51.33 pb^{-1} for e^+p collisions with a proton energy of 920 GeV and an $e^\pm$ energy of 27.5 GeV. This represents a factor ~ 30 increase over previously published HERA data [10, 20]. Since no dependence on the lepton charge is expected, the two data sets are combined[1]. The measurements are presented in the range $2 < Q^2 < 70\,\text{GeV}^2$ and $35 < W < 145\,\text{GeV}$.

2 Experimental set-up

A detailed description of the ZEUS detector can be found elsewhere [22]. A brief outline of the components that are most relevant for this analysis is given below.

Charged particles were reconstructed in the central tracking detector (CTD) [23] covering the polar-angle[2] region $15^\circ < \theta < 164^\circ$. The transverse-momentum resolution for full-length tracks is $\sigma(p_T)/p_T = 0.0058 p_T \oplus 0.0065 \oplus 0.0014/p_T$, with p_T in GeV.

The high-resolution uranium-calorimeter (CAL) [24] consists of three parts: the forward (FCAL), the barrel (BCAL) and the rear (RCAL) calorimeters. Each part is subdivided transversely into towers and longitudinally into an electromagnetic section (EMC) and either one (RCAL) or two (FCAL and BCAL) hadronic sections. The CAL covers 99.7% of the total solid angle. The energy resolution obtained from test-beam measurements was $\sigma(E)/E = 0.18/\sqrt{E}$ in the electromagnetic sections and $\sigma(E)/E = 0.35/\sqrt{E}$ in the hadronic sections, with E in GeV.

The forward plug calorimeter (FPC) [25] was a lead-scintillator sandwich calorimeter with readout via wavelength shifter fibers. It was installed in the beamhole of the FCAL and extended the pseudorapidity coverage of the forward calorimeter from $\eta \lesssim 4$ to $\eta \lesssim 5$.

The small-angle rear tracking detector (SRTD) [26] consists of two planes of scintillator strips read out via optical fibers and photomultiplier tubes. It is attached to the front face of the RCAL and covers an angular range between 4° and 18° around the beampipe. The SRTD provides a transverse position resolution of 0.3 cm [13] corresponding to an angular resolution of 2 mrad.

The hadron-electron separator installed in the RCAL (RHES) consists of silicon diodes placed at a longitudinal depth of three radiation lengths. The RHES provides an electron position resolution of 0.5cm if at least two adjacent pads are hit by the shower [27].

[1] Hereafter, both e^+ and e^- are referred to as electrons, unless explicitly stated otherwise.

[2] The ZEUS coordinate system is a right-handed Cartesian system, with the Z axis pointing in the proton beam direction, referred to as the "forward direction", and the X axis pointing left towards the centre of HERA. The coordinate origin is at the nominal interaction point.

The luminosity was determined from the rate of the bremsstrahlung process $ep \to e\gamma p$, where the photon was measured with a lead-scintillator calorimeter [28] located at $Z = -107$ m in the HERA tunnel.

3 Kinematics and cross sections

The following kinematic variables are used to describe exclusive ϕ production, $e(k)p(P) \to e(k')\phi(v)p(P')$, where k, k', P, P' and v are, respectively, the four-momenta of the incident electron, scattered electron, incident proton, scattered proton and the phi meson:

- $Q^2 = -q^2 = -(k - k')^2$, the negative four-momentum squared of the virtual photon;
- $W^2 = (q + P)^2$, the squared invariant mass of the photon-proton system;
- $y = (P \cdot q)/(P \cdot k)$, the fraction of the electron energy transferred to the proton in the proton rest frame;
- $x = Q^2/(2P \cdot q)$, the Bjorken variable;
- $t = (P - P')^2$, the squared four-momentum transfer at the proton vertex.

The kinematic variables were reconstructed with the "constrained" method [4] which uses the momentum of the ϕ and the polar and azimuthal angles of the scattered electron.

The ep cross section can be expressed in terms of the transverse, σ_T, and longitudinal, σ_L, virtual photoproduction cross sections as

$$\frac{d^2\sigma^{ep\to e\phi p}}{dydQ^2} = \Gamma_T(y, Q^2)\,(\sigma_T + \epsilon\sigma_L)\,,$$

where Γ_T is the flux of transverse virtual photons [29] and ϵ is the ratio of longitudinal and transverse virtual photon fluxes, given by $\epsilon = 2(1-y)/(1+(1-y)^2)$. In the kinematic range studied here, ϵ is in the range $0.975 < \epsilon < 1$, with an average value of 0.99.

The virtual photon-proton cross section, $\sigma^{\gamma^* p\to\phi p} \equiv \sigma_T + \epsilon\sigma_L$, can be used to evaluate the total exclusive cross section, $\sigma_{\rm tot}^{\gamma^* p\to\phi p} \equiv \sigma_T + \sigma_L$, through the relation

$$\sigma_{\rm tot}^{\gamma^* p\to\phi p} = \frac{1+R}{1+\epsilon R}\sigma^{\gamma^* p\to\phi p},$$

where $R = \sigma_L/\sigma_T$ is the ratio of the cross sections for longitudinal and transverse photons. The helicity structure of ϕ production is used to determine R as described in Section 7.6.1.

4 Reconstruction and selection of the events

The signature of exclusive ϕ electroproduction, $ep \to e\,\phi\,p$, consists of the scattered electron and two oppositely charged kaons from the ϕ decay. The scattered proton is deflected through a small angle and escapes undetected down the beampipe.

The events were selected online by a three-level trigger [30, 31]. The trigger required a scattered electron in the CAL with energy greater than 7 GeV, $2-5$ tracks in the CTD and a veto of $E < 5$ GeV in the inner ring of the FCAL.

The following criteria were applied offline to reconstruct and select the events:

- the identification and energy measurement of the scattered electron were provided by CAL. The energy was required to satisfy $E_e > 10$ GeV. The electron position was measured by three detectors: SRTD, HES and CAL. Given its superior resolution, high reliability and small biases the preference was given to the measurement from the SRTD. This was improved by the position obtained from HES or CAL when applicable. To ensure full containment of the electromagnetic shower and good position reconstruction, fiducial cuts were applied to the impact position of the electron on the face of the RCAL;
- the ϕ mesons were reconstructed from the decay kaons. No particle identification was used. Two tracks of opposite charge, well reconstructed in the CTD, with $p_T > 0.15$ GeV and $|\eta| < 1.7$, were selected and assigned the kaon mass. Additional CTD tracks associated with the scattered electron or kaon decays were allowed. Events with further tracks were rejected;
- the position of the reconstructed vertex was required to be compatible with that of an ep collision, $|z_{VTX}| < 50$ cm. The further requirement $r_{VTX} < 0.8$ cm was imposed, where r_{VTX} is the radial distance of the reconstructed vertex from the nominal beamline, to remove $K^0_S \to \pi^+\pi^-$ decays;
- to remove events with large initial-state radiation , the requirement $45 < E - p_z < 65$ GeV was imposed, where $E - p_z$ is summed over the two kaons and the scattered electron.
- to suppress non-exclusive events, the energy of each CAL cluster not associated to any of the final-state kaons or the scattered electron was required to be less than 0.3 GeV. To suppress further the contamination from proton-dissociative events, $ep \to e\phi Y$, the energy in the FPC was required to be less than 1 GeV. These cuts restrict the mass of the proton-dissociative system, Y, to $M_Y \lesssim 2.3$ GeV.

Requiring events to be in a kinematic region where the properties of the event are well measured, and further requiring that the acceptance only varies slowly with the kinematic variables, led to the following selection:

$$\begin{aligned} Q^2 &> 2\,\text{GeV}^2 \\ |t| &< 0.6\,\text{GeV}^2 \\ W &> 33.75\,\text{GeV} + 1.25\,\text{GeV}^{-1} \cdot Q^2 \\ W &< 100\,\text{GeV} + 37\,\text{GeV}^{-1} \cdot Q^2 \end{aligned}$$

with Q^2 given in GeV^2 in the last two expressions. The distribution of selected events in the x-Q^2 plane for $1.01 < m_{KK} < 1.04\,\text{GeV}$ is shown in Fig. 1.

5 Monte Carlo simulation

The acceptance and the effects of the detector response were determined using samples of Monte Carlo (MC) events. All generated events were passed through the standard ZEUS detector simulation, based on the GEANT 3.13 programme [32], and the ZEUS trigger simulation package.

The exclusive process $ep \to e\,\phi\,p$ was modelled using the ZEUSVM [33] MC generator interfaced to HERACLES 4.6.1 [34] to account for first-order QED radiative effects. The parameters describing the W, Q^2, t and helicity angle distributions in the MC were adjusted such that the MC reproduced the observed data distributions. The typical acceptance for $\phi \to K^+K^-$ was found to increase from 20% at $Q^2 = 2\,\text{GeV}^2$ to 60% for $Q^2 > 10\,\text{GeV}^2$.

Proton-dissociative events, $ep \to e\phi Y$, were modelled using the generator EPSOFT [35]. The $\gamma^*\,p \to \phi\,Y$ cross section was parametrised as

$$\frac{d^2\sigma^{\gamma^* p \to \phi Y}}{dt\ dM_Y^2} \propto f(Q^2, W) e^{-b|t|} M_Y^{-\beta} \tag{1}$$

with the same Q^2, W dependence as for the exclusive case and $b(Q^2) = 5.1/(1+R(Q^2))\,\text{GeV}^{-2}$ and $\beta = 2$ (see Section 6.2).

6 Extraction of the ϕ signal

Figure 2 shows the invariant-mass distribution of the K^+K^- pairs, obtained after the selection described in Section 4. A total of 4058 events were extracted in the mass range $1.01 < m_{KK} < 1.04\,\text{GeV}$ used for the cross section measurements. The natural width of the resonance is comparable to the detector resolution, which is 1.8 MeV for tracks at central rapidity, deteriorating to $\sim 5\,\text{MeV}$ for tracks crossing the CTD through large angles. The smooth non-resonant background is dominated by exclusive $\rho \to \pi^+\pi^-$ production.

6.1 Non-resonant background

The non-resonant background was estimated for each bin in which a cross section was extracted with unbinned likelihood fits to the invariant mass distribution. The assumed functional form was a p-wave relativistic Breit-Wigner convoluted with a gaussian resolution function for the signal plus a background function with the shape $a(m_{KK} - 2m_K)^b$. The background, estimated from the fit, is then subtracted from the number of observed events in the mass window. The contribution of the non-resonant background in the mass range of the signal is typically 18% at $Q^2 = 2.4\,\text{GeV}^2$, decreasing to 5% at $Q^2 = 13\,\text{GeV}^2$.

6.2 Proton-dissociative background

The remaining source of background consists of ϕ production accompanied by proton dissociation, $ep \to e\ \phi\ Y$, where the particles from the breakup of the proton are not detected. A similar study to that done for J/ψ production [13] was performed.

The fraction of proton-dissociative events in the final sample, averaged over t for $|t| < 0.6\,\text{GeV}^2$, was $f_{\text{p-diss}} = (7^{+10}_{-6})\%$, independent of W, Q^2 and helicity angles. The uncertainty is dominated by the uncertainty on the M_Y spectrum for $M_Y < 3\,\text{GeV}$. The fraction increases from 4.5% for $0 < |t| < 0.08\,\text{GeV}^2$ to 14.5% for $0.35 < |t| < 0.6\,\text{GeV}^2$. The cross sections presented in the next sections were corrected for this background in bins of t, and globally in W, Q^2 and helicity angle.

7 Results

7.1 Measurement of cross sections

In each bin of a kinematic variable, the ep cross section was extracted using the formula

$$\sigma^{ep\to e\ \phi\ p} = \frac{(N_{\text{data}} - N_{\text{bgd}})(1 - f_{\text{p-diss}})}{\mathcal{ABL}},$$

where N_{data} is the number of events in the data and N_{bgd} is the number of events from the non-resonant background. The overall acceptance is denoted as $\mathcal{A}$, $\mathcal{B}$ accounts for the ϕ decay branching ratio $(49.2 \pm 0.6)\%$ [36], and $\mathcal{L}$ is the integrated luminosity.

The total exclusive photon-proton cross section was calculated as

$$\sigma_{\text{tot}}^{\gamma^* p\to\phi p}(Q^2, W) = \sigma_{\text{tot,MC}}^{\gamma^* p\to\phi p}(Q^2, W) \cdot \frac{\sigma_{DATA}^{ep\to e\ \phi\ p}}{\sigma_{MC}^{ep\to e\ \phi\ p}}$$

In this way, the MC was used to correct for radiative effects, detector acceptance, cut efficiencies and the shape of the cross section within the bin.

The cross sections were measured for $|t| < 0.6\,\text{GeV}^2$. The results were then extrapolated to $|t| < \infty$ assuming $d\sigma/dt \propto e^{-b|t|}$. The correction factor needed to extrapolate to the cross section integrated over the full t range was evaluated bin-by-bin using the measured value of b for the given Q^2. The cross sections are quoted for the mass range $2m_K < m_{KK} < M_\phi + 5\Gamma$, where $M_\phi = 1019.4$ MeV and $\Gamma = 4.458$ MeV [36].

7.2 Systematic uncertainties

The systematic uncertainties on the measured cross sections were determined by varying the selection cuts and by modifying the analysis procedure. The sources of systematic uncertainties considered were similar to those of previously published analyses [13, 37].

The dominant sources of uncertainty are listed below. The size of the uncertainty for a given systematic effect depends on the cross section or parameter measured. Except for the two lowest Q^2 bins in the evaluation of $d\sigma/dQ^2$, the systematic uncertainties (excluding normalization uncertainty) were smaller than the statistical error.

- The electron position reconstruction is critical in determining the acceptance and in the kinematic variable reconstruction (via the 'constrained' method employed). Possible misalignments of the SRTD and CAL were estimated to be 2 mm, and the effect of such misalignments were tested via MC simulations. In addition, the electron fiducial cut was varied by 5 mm. These tests generally provided the largest source of uncertainty.

- The elasticity cut is important in suppressing non-exclusive events. Randomly triggered data events were used to estimate the effects of calorimeter noise and the noise was implemented in the MC simulation. The energy distribution of the most energetic cluster not assigned to the electron or one of the kaons was compared in data and MC. The MC simulation was found to reproduce the data distributions well, indicating a very small non-exclusive contribution with extra particles in the central region. The cut was varied from 0.3 to 0.4 GeV in both data and MC to investigate residual uncertainties.

- The stability of the fitting procedure and extraction of the signal was checked by reducing the fit range to $m_{KK} < 1.07\,\text{GeV}$ and changing the accepted mass range to $1.01 < m_{KK} < 1.035\,\text{GeV}$ respectively. Except for the bins with lowest statistics the contribution to the overall uncertainty is small.

- Uncertainties from the dependence on the MC parametrisations were also estimated and found to be small as compared to other sources of systematical errors.

- The normalization uncertainty was different for different measurements. All measurements had a normalization uncertainty due to uncertainties in the integrated luminosity, $\pm 2.5\%$, and due to the uncertainty in the decay branching ratio, $\pm 1.2\%$ leading to a combined uncertainty of $\pm 2.8\%$. In the case of the $d\sigma/dQ^2$ and $d\sigma/dW$ measurements, the proton dissociation is subtracted globally and the normalization uncertainty is increased to $+10.4\% - 6.6\%$. The uncertainty due to the subtraction of proton-dissociative background for the $d\sigma/dt$ measurement resulted in a t-dependent uncertainty as discussed in Section 6.2. For the angular distributions, the normalization uncertainty does not appear as only the shapes of the distributions, $\frac{1}{\sigma}\frac{d\sigma}{dcos(\theta_h)}$, were measured.

The total systematic uncertainty (excluding the normalization uncertainty) was determined by adding the individual contributions in quadrature. The correlated and uncorrelated systematic uncertainties were evaluated separately. The typical size of the systematic uncertainty (except normalization) was 5% for the cross sections in W and Q^2 bins, and 5% at small $|t|$ increasing to 10% at $|t| = 0.6\,\text{GeV}^2$.

7.3 Dependence on W and Q^2

The cross section $\sigma_{\text{tot}}^{\gamma^* p \to \phi p}$, measured as a function of W and Q^2, is shown in Fig. 3 (top). The data were fitted to a dependence $\sigma \propto W^\delta$, with $\delta \approx 0.3$. The fitted values of δ are compared to those from previous ZEUS measurements for different VM in Fig. 3 (bottom). The behavior of δ is consistent with a scaling of the W dependence for exclusive VM production with $Q^2 + M_V^2$.

The Q^2 dependence of the cross section is shown in Fig. 4 for $W = 75\,\text{GeV}$, compared to previous ZEUS and H1 results. The ϕ data from this analysis was fit to a dependence of the form $\sigma \propto (Q^2 + M_\phi^2)^{-n}$. The higher precision data from this analysis reveal that the full dependence cannot be fitted with a single value of n for the full Q^2 range. There are several possible causes which could lead to this behavior, including the variation of R with Q^2, the dependence of α_S on Q^2 and the changing Q^2 dependence of the gluon density at fixed W.

7.4 Dependence on t

The differential cross section, $d\sigma^{\gamma^* p \to \phi p}/dt$, measured as a function of t in the range $|t| < 0.6\,\text{GeV}^2$, is shown in Fig. 5 (top) for different values of Q^2. The data have been centered at $W = 75\,\text{GeV}$. A function of the form $d\sigma/dt = d\sigma/dt|_{t=0} \cdot e^{-b|t|}$ was fitted to the data and the results of the fit are given in Fig. 5 (bottom), along with measurements from other VMs. The ϕ measurements are consistent with a global $Q^2 + M_V^2$ dependence for the slope parameter b.

7.5 Pomeron trajectory

Soft diffractive processes are described by Regge phenomenology [2] in terms of the exchange of a Pomeron trajectory. In hard interactions, where Regge phenomenology may not be applicable, an effective Pomeron trajectory may nevertheless be extracted. The data sample was analyzed to determine the effective Pomeron trajectory. In the Regge formalism, the differential cross section can be expressed as

$$d\sigma/dt \propto W^{4(\alpha_{I\!P}(t)-1)}, \tag{2}$$

where the trajectory $\alpha_{I\!P}$ is usually parametrised as

$$\alpha_{I\!P}(t) = \alpha_{I\!P}(0) + \alpha'_{I\!P}t. \tag{3}$$

In this notation, $\alpha_{I\!P} = 1+\delta/4$. The effective Pomeron trajectory was determined by fitting Eq. (2) to the differential cross sections at different t values. The fit was performed in five t bins at $Q^2 = 5\,\text{GeV}^2$. Since the proton-dissociative process has the same W dependence as the exclusive process, the extraction of $\alpha_{I\!P}$ is not sensitive to this background contribution, which populates the high-t region. Therefore the analysis was extended up to $|t| = 1\,\text{GeV}^2$. The fit results are shown in Fig. 6 (top). The parameters of the trajectory were determined from a fit of Eq.(3) to the extracted $\alpha_{I\!P}(t)$ values, as shown in Fig. 6 (bottom).

The results are in agreement with the ZEUS results from J/ψ production [3, 13] but are not consistent with the trajectory measured in soft diffractive processes, $\alpha_{I\!P} = 1.08 + 0.25\,t$ [38, 39]; i.e., no t-dependence is observed.

7.6 Decay angular distributions

The study of the angular distributions of the decay of the ϕ provides information about the photon and ϕ polarization states. In the helicity frame [40], the production and decay of the ϕ can be described in terms of three angles: Φ_h, the angle between the ϕ production plane and the lepton scattering plane; θ_h, the polar angle, and ϕ_h, the azimuthal angle of the positively charged kaon. Under the assumption of s-channel helicity conservation (SCHC), the normalised angular distribution depends only on two angles, θ_h and $\psi_h = \phi_h - \Phi_h$. The θ_h distribution can be expressed in the form

$$\frac{1}{N}\frac{dN}{d\cos\theta_h} = \frac{3}{8}\left[1 + r_{00}^{04} + (1 - 3r_{00}^{04})\cos^2\theta_h\right] \tag{4}$$

The spin-density matrix element r_{00}^{04} represents the probability that the ϕ is produced in the helicity-0 state from a virtual photon of helicity 0 or 1.

The normalized cross section $\frac{1}{\sigma}\frac{d\sigma^{\gamma^* p\to\phi p}}{dcos(\theta_h)}$ at $W = 90$ GeV is shown in Fig. 7 for seven values of Q^2 and $W = 90$ GeV. Equation (4) was fitted to the data. The values of r_{00}^{04}, determined from the fits, are plotted in Fig. 8 (top) and compared to the values extracted for other VMs. In this case, a global scaling of r_{00}^{04} with Q^2/M_V^2 is observed.

7.6.1 Longitudinal and transverse cross sections

The ratio of the longitudinal to transverse cross section, $R = \sigma_L/\sigma_T$, was calculated as a function of Q^2 from r_{00}^{04} according to the relation

$$R = \frac{1}{\epsilon}\frac{r_{00}^{04}}{1 - r_{00}^{04}},$$

which is valid under the assumption of SCHC[3]. The average value of $\epsilon = 0.99$ was used in extracting R.

The values of R as a function of Q^2 are compared with previous ZEUS and H1 results [9] in Fig. 8 (bottom). They are well described by the expression $R = a(Q^2/M_\phi^2)^b$. The parameters were extracted from the fit to r_{00}^{04} data for which the statistical errors are gaussian, yielding $a = 0.51 \pm 0.07(\text{stat.}) \pm 0.05(\text{syst.})$ and $b = 0.86 \pm 0.11(\text{stat.}) \pm 0.05(\text{syst.})$.

8 Summary

The exclusive electroproduction of ϕ mesons, $ep \to e\phi\, p$, has been measured with the ZEUS detector at HERA for photon virtualities in the range $2 < Q^2 < 70\,\text{GeV}^2$, for photon-proton centre-of-mass energies in the range $35 < W < 145$ GeV and for four-momentum-transfer squared in the range $|t| < 0.6\,\text{GeV}^2$. The extracted $\gamma^* p$ cross section rises with W as $\sigma \propto W^\delta$, with a slope parameter $\delta \approx 0.3$. This parameter changes slowly with Q^2 and is consistent with that observed from other VM when scaled as $Q^2 + M_V^2$.

The t distribution, measured for $|t| < 0.6\,\text{GeV}^2$, is well described by an exponential dependence over the range $2 < Q^2 < 70\,\text{GeV}^2$. The slope parameter, b, is consistent with a scaling of b with $Q^2 + M_V^2$.

An analysis of the cross sections in the framework of Regge phenomenology yields an effective Pomeron trajectory consistent with that measured in J/ψ production; i.e., no t-dependence is observed.

[3] The validity of SCHC has been tested for other VMs and found to be adequate for the purpose of extracting R [15].

The ratio of the cross sections for longitudinally and transversely polarized photons, R, increases with Q^2 and the increase becomes less rapid with larger values of Q^2. The results are consistent with a scaling with Q^2/M_V^2.

Acknowledgements

We thank the DESY directorate for their strong support and encouragement. The special effort of the HERA group is gratefully acknowledged. We are grateful for the support of the DESY computing and network services. The design, construction and installation of the ZEUS detector has been made possible by the efforts and ingenuity of many people who are not listed as authors.

References

[1] S.J. Brodsky et al., Phys. Rev. **D 50**, 3134 (1994).

[2] P.D.B. Collins, *An Introduction to Regge Theory and High Energy Physics*. Cambridge University Press, 1977.

[3] ZEUS Coll., S. Chekanov et al., Preprint Hep-ex/0404008, 2004.

[4] ZEUS Coll., J. Breitweg et al., Eur. Phys. J. **C 6**, 603 (1999).

[5] H1 Coll., C. Adloff et al., Eur. Phys. J. **C 13**, 371 (2000).

[6] H1 Coll., C. Adloff et al., Phys. Lett. **B 539**, 25 (2002).

[7] ZEUS Coll., M. Derrick et al., Z. Phys. **C 73**, 73 (1996).

[8] ZEUS Coll., J. Breitweg et al., Phys. Lett. **B 487**, 273 (2000).

[9] H1 Coll., C. Adloff et al., Eur. Phys. J. **C 10**, 373 (1999).

[10] H1 Coll., C. Adloff et al., Phys. Lett. **B 483**, 23 (2000).

[11] ZEUS Coll., J. Breitweg et al., Phys. Lett. **B 437**, 432 (1998).

[12] H1 Coll., C. Adloff et al., Phys. Lett. **B 541**, 251 (2002).

[13] ZEUS Coll., S. Chekanov et al., Eur. Phys. J. **C 24**, 345 (2002).

[14] ZEUS Coll., J. Breitweg et al., Eur. Phys. J. **C 2**, 247 (1998).

[15] ZEUS Coll., J. Breitweg et al., Eur. Phys. J. **C 12**, 393 (2000).

[16] ZEUS Coll., *Exclusive electroproduction of ρ^0 mesons with the ZEUS detector at HERA*. Abstract 880, International Europhysics Conference on High Energy Physics, Budapest, Hungary, July 2000, 2001.

[17] ZEUS Coll., *Exclusive electroproduction of ρ^0 mesons at HERA*. Abstract 594, International Europhysics Conference on High Energy Physics, Budapest, Hungary, July 2001, 2001.

[18] ZEUS Coll., *Exclusive and proton-dissociative electroproduction of ρ^0 mesons at HERA*. Abstract 818, International Conference on High Energy Physics, Amsterdam, July 2002, 2002.

[19] ZEUS Coll., M. Derrick et al., Phys. Lett. **B 377**, 259 (1996).

[20] ZEUS Coll., M. Derrick et al., Phys. Lett. **B 380**, 220 (1996).

[21] M. Groll, *Electroproduction of ϕ mesons at $0.25 < Q^2 < 0.85 GeV^2$ at HERA*. Diplom Thesis, Hamburg University, Report DESY-THESIS-1998-008, 1998, 1998.

[22] ZEUS Coll., U. Holm (ed.), *The ZEUS Detector*. Status Report (unpublished), DESY (1993), available on `http://www-zeus.desy.de/bluebook/bluebook.html`.

[23] N. Harnew et al., Nucl. Inst. Meth. **A 279**, 290 (1989);
B. Foster et al., Nucl. Phys. Proc. Suppl. **B 32**, 181 (1993);
B. Foster et al., Nucl. Inst. Meth. **A 338**, 254 (1994).

[24] M. Derrick et al., Nucl. Inst. Meth. **A 309**, 77 (1991);
A. Andresen et al., Nucl. Inst. Meth. **A 309**, 101 (1991);
A. Caldwell et al., Nucl. Inst. Meth. **A 321**, 356 (1992);
A. Bernstein et al., Nucl. Inst. Meth. **A 336**, 23 (1993).

[25] ZEUS Coll., FPC group, A. Bamberger et al., Nucl. Inst. Meth. **A 450**, 235 (2000).

[26] A. Bamberger et al., Nucl. Inst. Meth. **A 401**, 63 (1997).

[27] A. Dwurazny et al., Nucl. Inst. Meth. **A 277**, 176 (1989).

[28] J. Andruszków et al., Acta Phys. Pol. **B 32**, 2025 (2001).

[29] L.N. Hand, Phys. Rev. **129**, 1834 (1963).

[30] W.H. Smith, K. Tokoshuku and L.W . Wiggers, *Proc.Computing in High-Energy Physics (CHEP), Annecy, France*, C. Verkerk and W. Wojcik (eds.), p. 222. (1992). Also in preprint DESY 92-150B.

[31] W.H. Smith et al., Nucl. Inst. Meth. **A 355**, 278 (1995).

[32] R. Brun et al., GEANT3, Technical Report CERN-DD/EE/84-1, CERN, 1987.

[33] K. Muchorowski. Ph.D. Thesis, Warsaw University, 1996.

[34] A. Kwiatkowski, H. Spiesberger and H.-J. Möhring, Comp. Phys. Comm. **69**, 155 (1992). Also in *Proc. Workshop Physics at HERA*, Ed. W. Buchmüller and G.Ingelman, (DESY, Hamburg, 1991);
H. Spiesberger, *An Event Generator for ep Interactions at HERA Including Radiative Processes (Version 4.6)*, 1996, available on `http://www.desy.de/~hspiesb/heracles.html`.

[35] L. Adamczyk, *Vector Meson Photoproduction at Large Momentum Transfer at HERA*. Ph.D. Thesis, University of Mining and Metallurgy, Cracow, Poland, Report DESY-THESIS-1999-045, DESY, 1999;
M. Kasprzak, *Inclusive Properties of Diffractive and Non-diffractive Photoproduction at HERA*. Ph.D. Thesis, Warsaw University, Warsaw, Poland, Report DESY F35D-96-16, DESY, 1996.

[36] Particle Data Group, K. Hagiwara et al., Phys. Rev. **D 66**, 010001 (2002).

[37] ZEUS Coll., S. Chekanov et al., Eur. Phys. J. **C 21**, 443 (2001).

[38] A. Donnachie and P.V. Landshoff, Phys. Lett. **B 348**, 213 (1995).

[39] G.A. Jaroszkiewicz and P.V. Landshoff, Phys. Rev. **D 10**, 170 (1974).

[40] K. Schilling and G. Wolf, Nucl. Phys. **B 61**, 381 (1973).

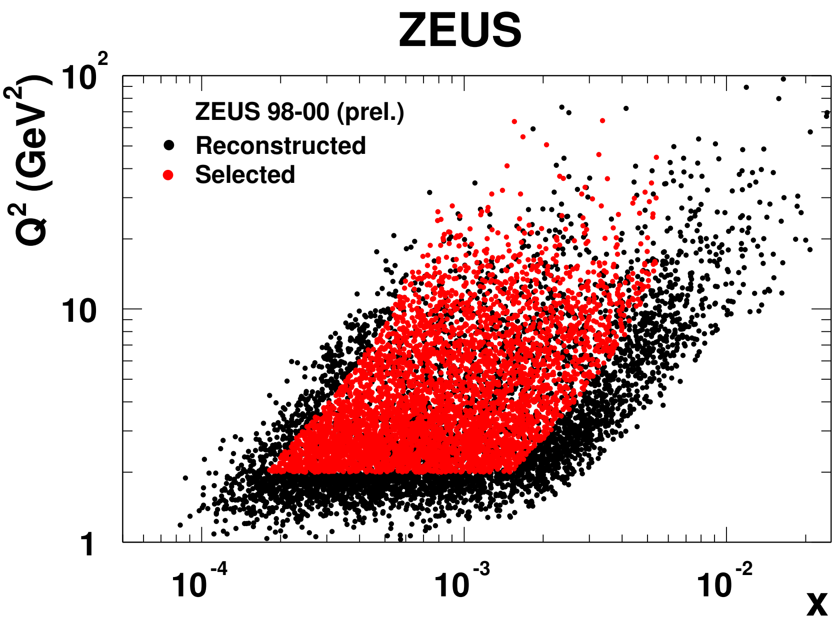

Figure 1: *The distribution of the events in the kinematic plane of Bjorken-x and Q^2. The black dots represent all reconstructed events while the red dots are events in the accepted kinematic range (Section 4).*

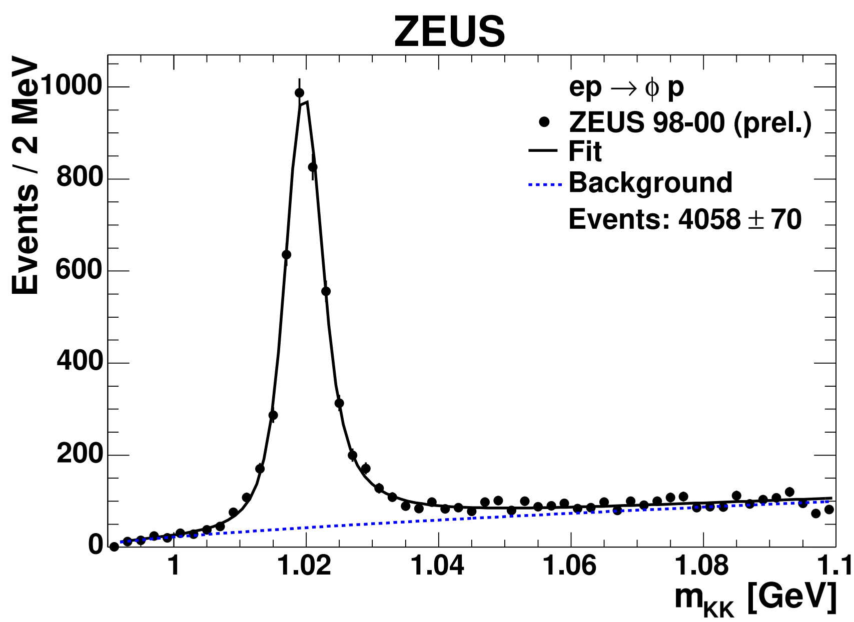

Figure 2: *Invariant mass distribution of the K^+K^- candidate pairs. The solid line shows the result of a fit including signal+background, while the dotted line shows the background component only. The error bars indicate the statistical uncertainties.*

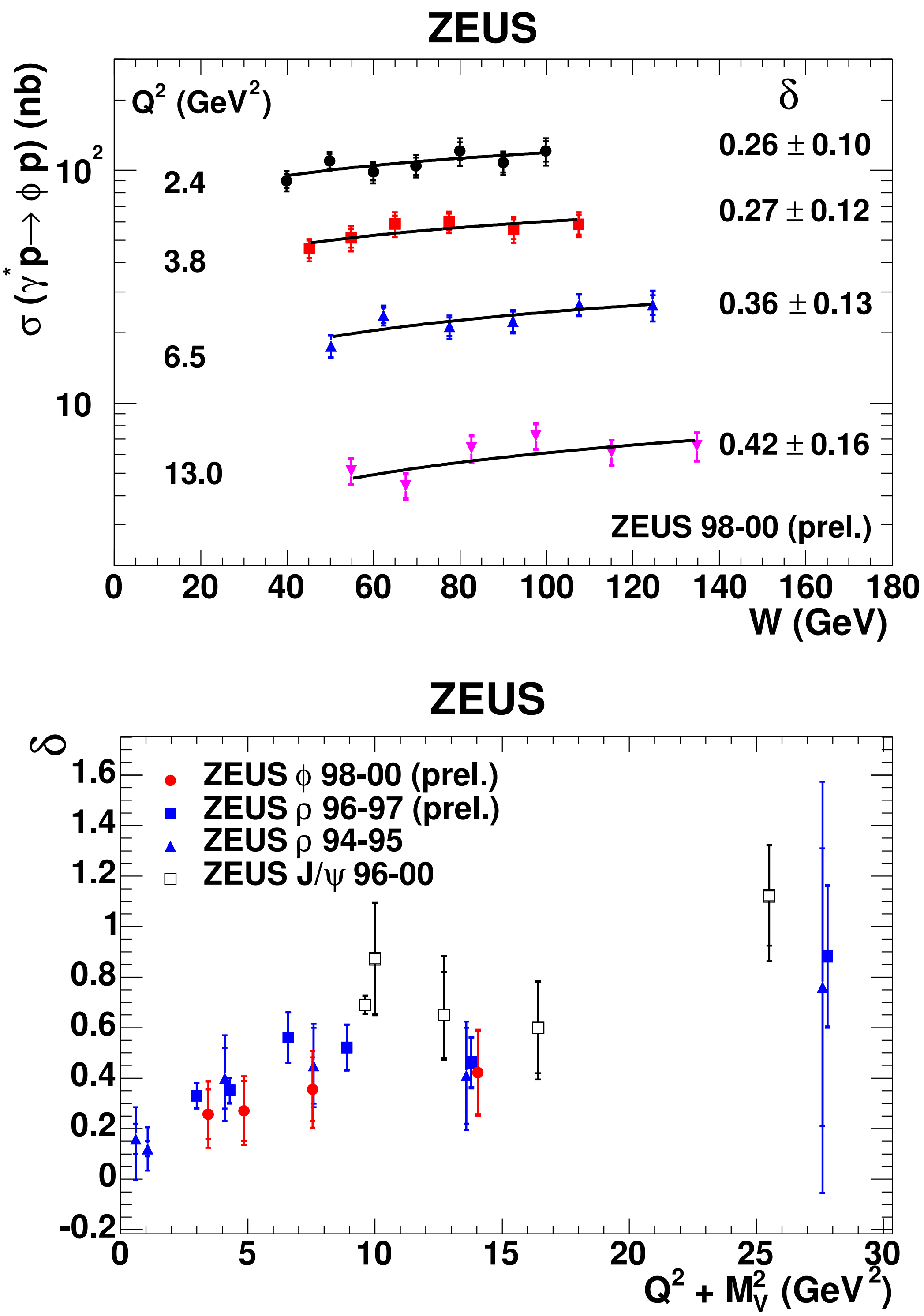

Figure 3: *(top) Exclusive ϕ cross section as a function of W for four values of Q^2. The solid lines are a result of a fit to the form $\sigma \propto W^\delta$. (bottom) Extracted values of δ compared with results from other VMs. The inner error bars represent the statistical uncertainties, while the outer error bars represent the quadratic sum of the statistical and systematic uncertainties. The overall normalization uncertainty of $^{+10.4}_{-6.6}$% is not included in the error bar in the upper plot.*

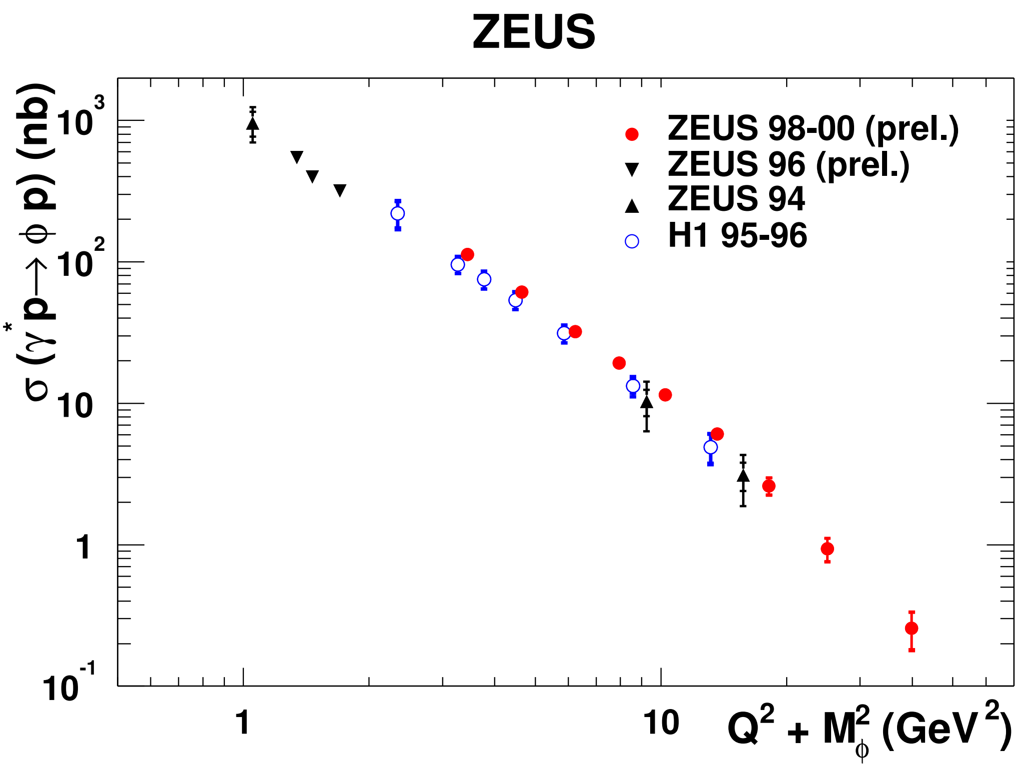

Figure 4: *Exclusive ϕ cross section as a function of Q^2 for $W = 75\,GeV$. The inner error bars represent the statistical uncertainties, while the outer error bars represent the quadratic sum of the statistical and systematic uncertainties. The overall normalization uncertainties are not shown. For the ϕ data of this analysis, it is $^{+10.4}_{-6.6}\%$.*

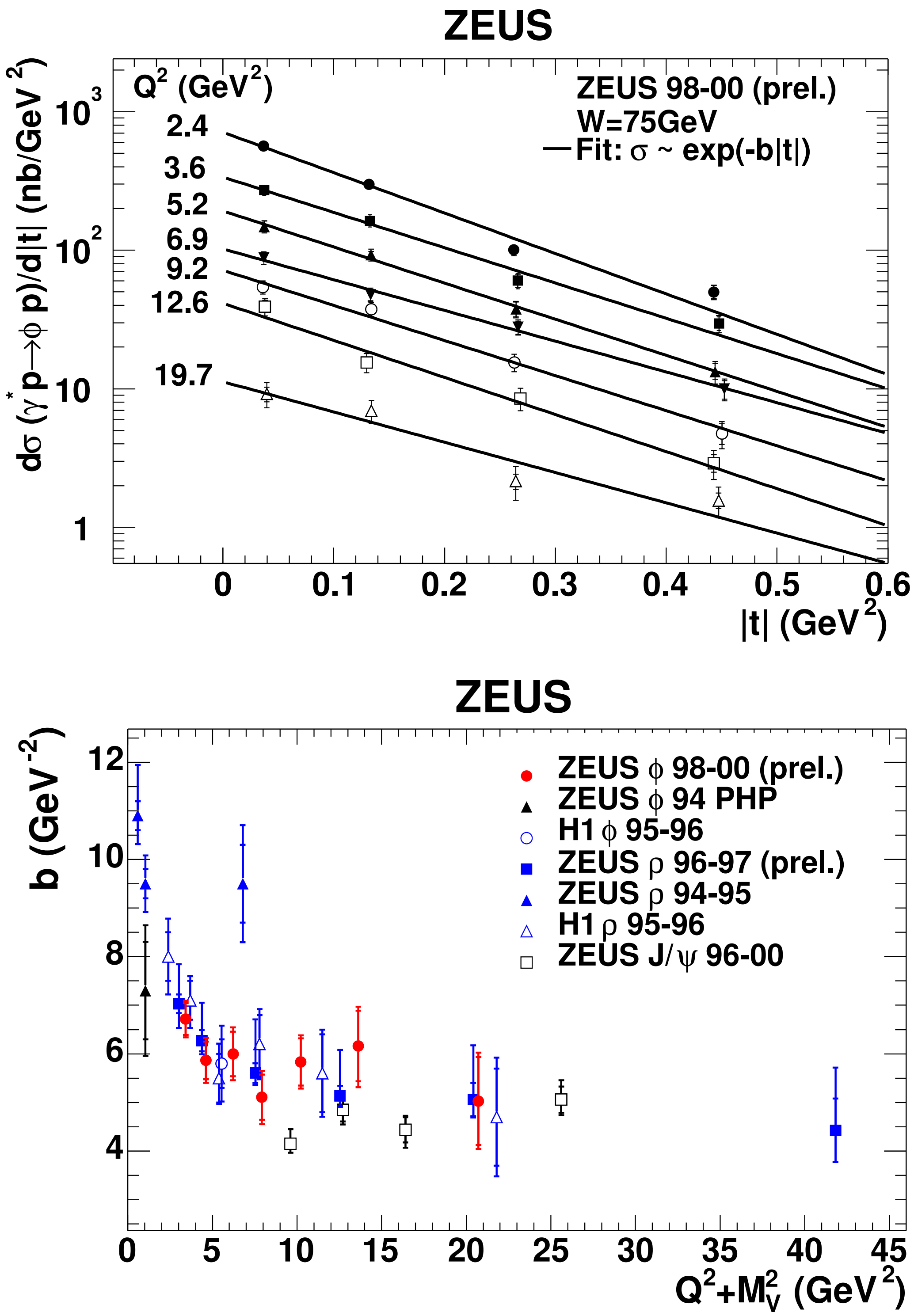

Figure 5: *(top) Differential cross-sections $d\sigma/dt$ for seven bins of Q^2, for $W = 75\,GeV$ and $|t| < 0.6\,GeV^2$. The full lines are the results of fits to the form $d\sigma/dt = d\sigma/dt|_{t=0} \cdot e^{-b|t|}$. (bottom) The slope b, as a function of $Q^2 + M_V^2$, compared to previous ZEUS and H1 results. The inner error bars represent the statistical uncertainty, the outer bars the statistical and systematic uncertainties added in quadrature. The overall normalization uncertainty of 2.8 % is not included in the error bar in the upper plot.*

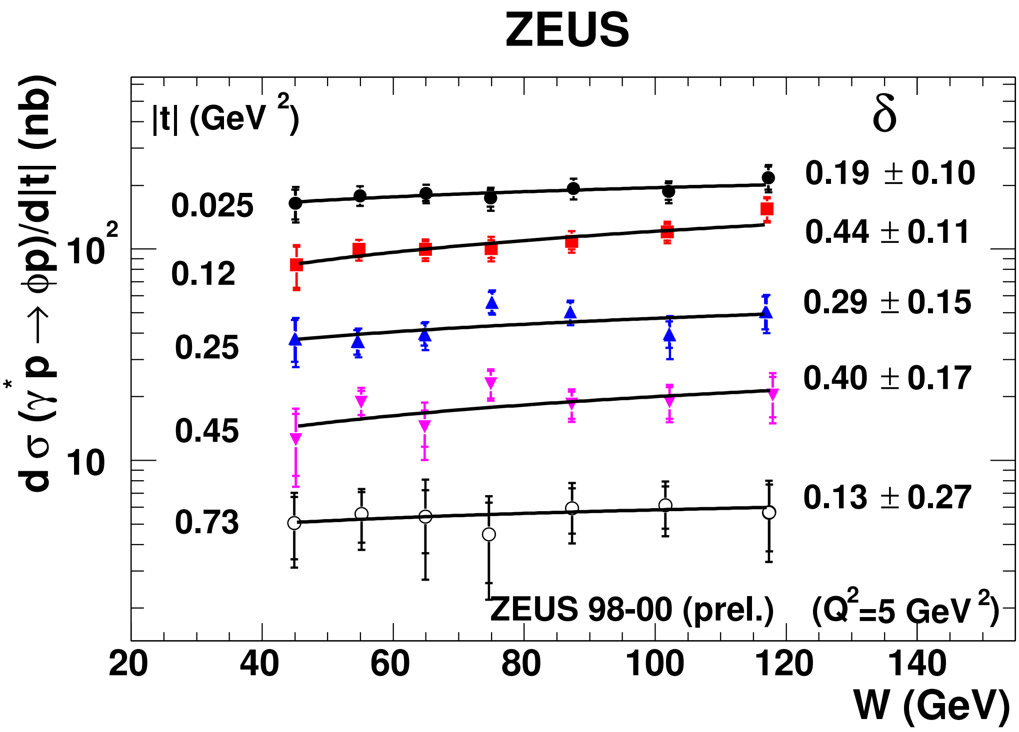

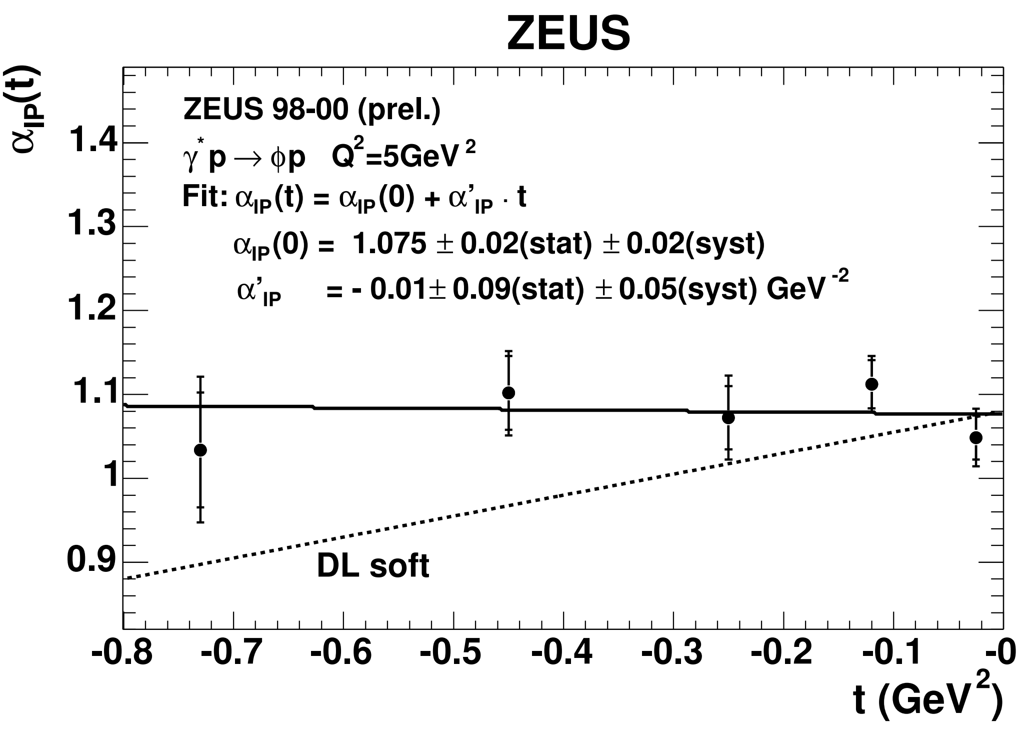

Figure 6: *(top) Differential cross sections $d\sigma/dt$ as a function of W for different values of $|t|$ and $Q^2 = 5$ GeV^2; the full lines are fits to W^δ. The mean contribution from proton dissociation has been subtracted. The normalization uncertainty is not included in the plot. (bottom) The full line is a linear fit to $\alpha_{I\!P} = 1 + \delta/4$ with the form given in Eq.(3). The dotted line is the soft Pomeron trajectory [38]. The inner error bars represent the statistical uncertainty, the outer bars the statistical and systematic uncertainties added in quadrature.*

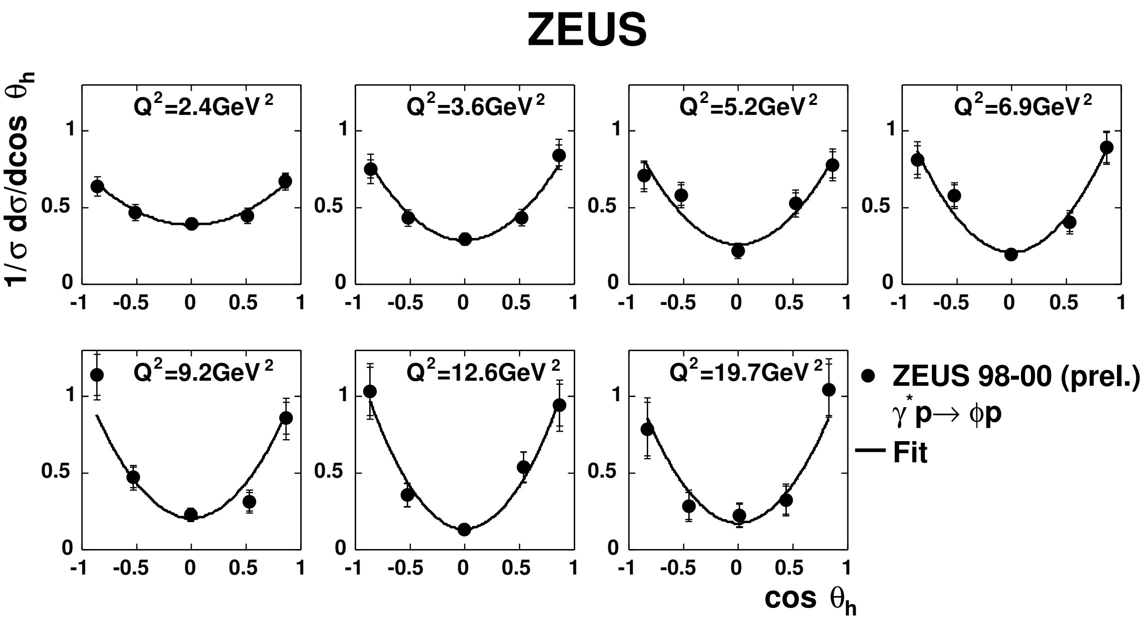

Figure 7: *Normalized distributions of $\cos\theta_h$ in seven Q^2 bins; the curves are the fits to Eq. (4). The inner error bars represent the statistical uncertainty, the outer bars the statistical and systematic uncertainties added in quadrature.*

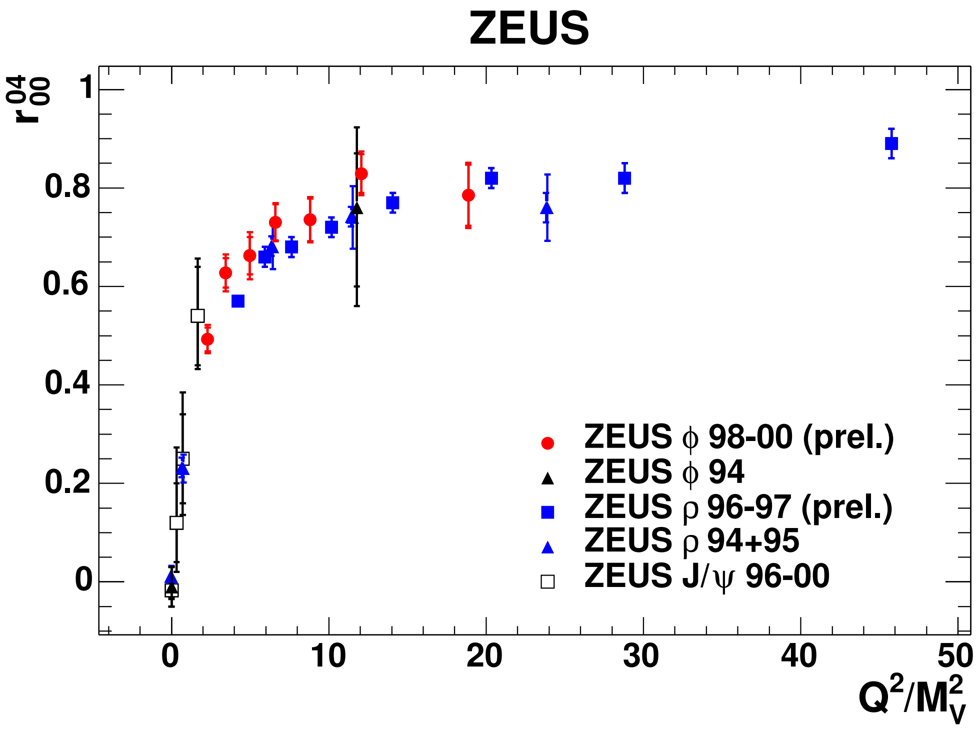

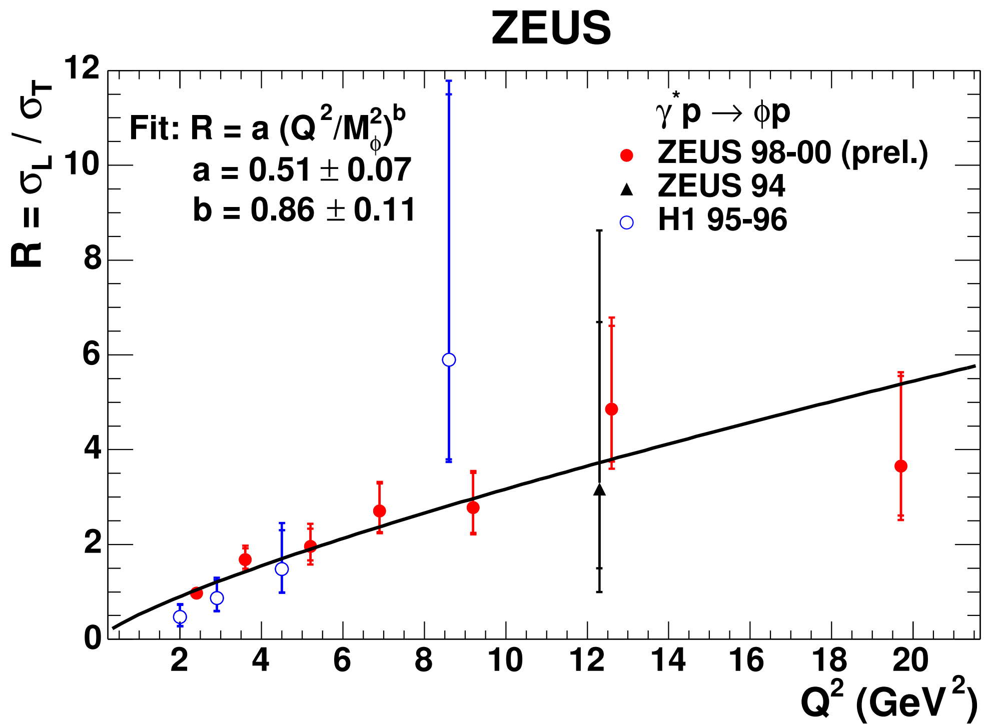

Figure 8: *(top) The value of r_{00}^{04} extracted from the fits shown in Fig. 7 plotted as a function of Q^2/M_V^2 compared with values for other VMs. Scaling with Q^2/M_V^2 is observed. (bottom) Ratio $R = \sigma_L/\sigma_T$ as a function of Q^2; the full line is the result of the two-parameter fit as shown in the plot. The error bars are statistical (inner) and total (outer).*